Applied Surface Science 330 (2015) 262–269

Contents lists available at ScienceDirect

Applied Surface Science

journal homepage: www.elsevier.com/locate/apsusc

Aragonite coating solutions (ACS) based on artificial seawater

A. Cuneyt Tas*

Department of Materials Science and Engineering, University of Illinois, Urbana, IL 61801, USA

ARTICLE INFO

Article history:
Received 27 October 2014
Received in revised form
30 December 2014
Accepted 30 December 2014
Available online 7 January 2015

Keywords:
Aragonite
Coating
Biomimicry
Artificial
Seawater

ABSTRACT

Aragonite ($CaCO_3$, calcium carbonate) is an abundant biomaterial of marine life. It is the dominant inorganic phase of coral reefs, mollusc bivalve shells and the stalactites or stalagmites of geological sediments. Inorganic and initially precipitate-free aragonite coating solutions (ACS) of pH 7.4 were developed in this study to deposit monolayers of aragonite spherules or ooids on biomaterial (*e.g.*, UHMWPE, ultrahigh molecular weight polyethylene) surfaces soaked in ACS at 30 °C. The ACS solutions of this study have been developed for the surface engineering of synthetic biomaterials. The abiotic ACS solutions, enriched with calcium and bicarbonate ions at different concentrations, essentially mimicked the artificial seawater composition and started to deposit aragonite after a long (4 h) incubation period at the tropical sea surface temperature of 30 °C. While numerous techniques for the solution deposition of calcium hydroxyapatite ($Ca_{10}(PO_4)_6(OH)_2$), of low thermodynamic solubility, on synthetic biomaterials have been demonstrated, procedures related to the solution-based surface deposition of high solubility aragonite remained uncommon. Monolayers of aragonite ooids deposited at 30 °C on UHMWPE substrates soaked in organic-free ACS solutions were found to possess nano-structures similar to the mortar-and-brick-type botryoids observed in biogenic marine shells. Samples were characterized using SEM, XRD, FTIR, ICP-AES and contact angle goniometry.

1. Introduction

Aragonite ($CaCO_3$) is an abundant inorganic phase of marine biomineralization and geological dripstones (*e.g.*, stalactites and stalagmites) or various sedimentary formations [1–3]. The inorganic part of mollusc bivalve shells (clams, oysters, scallops and mussels), gastropods (snails), coral reefs and mother-of-pearl (nacre) is comprised of aragonite crystals stacked in a mortar-and-brick manner.

Aragonite (P*nam* (Hermann–Mauguin No. 62), orthorhombic), calcite (R-3*c* (167), rhombohedral), and vaterite (P6_3/*mmc* (194), hexagonal) are the anhydrous crystalline polymorphs of calcium carbonate. Hydrated and X-ray-amorphous calcium carbonate (ACC), on the other hand, can be formed as a precursor phase in some $CaCO_3$ syntheses [4,5]. Calcite is the most abundant and stable polymorph of calcium carbonate on earth, while vaterite (μ-$CaCO_3$), named after Heinrich Vater [6], is the least abundant among the three anhydrous polymorphs. Plummer and Busenberg [7] reported the solubility products (*i.e.*, $\log K_{SP}$ values) of calcite (−8.48 at 25 °C and −8.56 at 37 °C), aragonite (−8.33 at 25 °C and −8.40 at 37 °C) and vaterite (−7.91 at 25 °C and −8.05 at 37 °C) in water; therefore, aragonite has a slightly higher solubility than that of calcite.

While the synthetic $CaCO_3$ powders, usually of the calcite form, have found widespread use in cosmetics, food, toothpaste, plastics, paper-making, ink, paint, textile, pharmaceutical, and rubber industries, the crystallization of aragonite in seawater (instead of distilled water) for carbon sequestration remains as a developing area of research [8]. Despite significant research concentrating on the physical–chemical characterization of the mortar-and-brick-type aragonite of molluscan nacre, studies on the biomimetic synthesis of aragonite in artificial (or natural) seawater, in lieu of distilled/deionized water, and simultaneously at the sea surface temperature have either been limited or focused on calcite crystallization in seawater [9–20]. The objective of the current study is to contribute to this field of completely inorganic and biomimetic synthesis performed in artificial seawater (ASW). A significant number of non-biomimetic techniques have been suggested for synthesizing aragonite in distilled water, just to cite a few here, by Bragg [21], Backstrom [22], Wray and Daniels [23], Bills [24], Ota et al. [25], Wang et al. [26], Ahn et al. [27], Thachepan et al. [28], Park et al. [29], Beck and Andreassen [30], Sand et al. [31], and Jiang et al. [32].

* Tel.: +1 217 344 6708; fax: +1 217 333 2736.
E-mail address: c_tas@hotmail.com
URL: http://www.cuneyttas.com.

http://dx.doi.org/10.1016/j.apsusc.2014.12.195
0169-4332/

Artificial seawater (ASW) was formulated by Kester et al. [33] in 1967, as a revision to the 1940 recipe of Lyman and Fleming [34], and later evolved into an ASTM standard (D1141-98) [35]. The composition of ASW [33–35], together with the compositions of the novel solutions of this study, are presented in the following chapter. Briefly, ASW is an aqueous solution rich in Mg^{2+} and SO_4^{2-}; with a Mg^{2+}/Ca^{2+} molar ratio of 5.34 and a SO_4^{2-}/Ca^{2+} ratio of 2.82 [33–35]. ASW can also be obtained from a number of commercial vendors. On the other hand, the phosphate ion (PO_4^{3-}) concentration at the surface of seas and oceans is around 0.8 nM (nanomolar) and it can only increase to values ranging from 1.6 to 2.4 μM at depths of 1–3 km [36]. This deficiency of PO_4^{3-} ions makes it difficult to observe calcium phosphate crystallization in seas and oceans.

Electrochemically-polarized steel electrodes immersed in artificial [36–40] or natural [41] seawater were found to form crystalline calcareous deposits (scale) of aragonite, but not calcite, on their surfaces. The above electrochemical studies [36–41] inspired the current study and a number of aragonite coating solutions (ACS) are presented here which are completely inorganic, precipitate-free, and capable of forming aragonite, *in situ*, only upon heating to the typical tropical sea surface temperature of 30 °C [42,43], following 4 h of an incubation time at 30 °C.

SBF (simulated [44] or synthetic [45,46] body fluid) solutions, containing Ca^{2+}, Mg^{2+}, K^+, Na^+, HPO_4^{2-}, HCO_3^-, SO_4^{2-} and Cl^-, mimic the inorganic electrolyte composition of blood plasma, and were shown to deposit spherules of bone mineral-like carbonated apatitic calcium phosphate on immersed substrates when heated at the physiological temperature of 37 °C. On the other hand, Pan et al. [47] provided a careful clarification on why SBF solutions would not be suitable to predict the bioactivity of synthetic biomaterials immersed in those. The abiotic ACS solutions of this study mimic the liquid in which the inorganic phase (aragonite) of coral reefs or mollusc shells are forming.

ACS solutions described here may be useful to deposit high solubility aragonite, rather than low solubility Ca-hydroxyapatite ($\log K_{SP}$ being equal to −117.1) of SBFs, on the surfaces of porous or non-porous polymeric, metallic or ceramic implantable materials to modify their biocompatibility. The current demonstration of ACS solutions may also contribute to the broader carbon sequestration research to be performed in large quantities of seawater.

2. Materials and methods

2.1. Aragonite coating solutions (ACS)

High-purity (>99.9% pure) inorganic salts of Table 1 were added one by one, in the order given, to 500 mL of pre-boiled deionized water to prepare ACS solutions in sterile glass beakers. Precipitate-free ACS solutions had the autogenic pH (Orion Star 215 pH-meter, Thermo Scientific, USA) of 7.4 ± 0.06 at the time of preparation at room temperature (RT, 22 ± 1 °C). ASW (artificial seawater [35]) was also prepared as shown in Table 1. Static coating experiments were performed (for 48 h) at 30 °C in sealed high-density polyethylene (HDPE) bottles. A new HDPE bottle was used for each experiment and the experiments were repeated thrice.

Each crystallization bottle contained four pieces (10 mm × 10 mm × 1 mm) of ultrahigh molecular weight polyethylene (UHMWPE) coupons (DSM Medical, Netherlands) laid flat at the bottom. UHMWPE is the polymeric material used in various total knee and hip replacement implants. The coupons were washed with deionized water at the end of experiments, followed by dehydration in pure ethanol, and dried at RT for 36 h.

The ionic strength (I) of a biomineralization solution, such as ACS-2, is calculated as shown in Eq. (1), using the formula of Debye and Hückel [48]. One simply enters into the below formula the concentrations of ions (in M, moles/L) and the valency of ions. The value of the ionic strength (expressed in molarity, M) then serves as a reliable numerical index to exchange between researchers using and/or developing different biomineralization media based on their specific research needs.

$$\begin{aligned} I = \tfrac{1}{2}[&\overset{Ca^{2+}}{(18.72\times10^{-3})(2)^2} + \overset{Na^{+}}{(510.48\times10^{-3})(1)^2} + \overset{F^{-}}{(0.7\times10^{-4})(1)^2} \\ &+ \overset{Cl^{-}}{(576.26\times10^{-3})(1)^2} + \overset{HCO_3^{-}}{(32.81\times10^{-3})(1)^2} + \overset{K^{+}}{(10.15\times10^{-3})(1)^2} \\ &+ \overset{Mg^{2+}}{(54.6\times10^{-3})(2)^2} + \overset{SO_4^{2-}}{(28.8\times10^{-3})(2)^2} + \overset{Br^{-}}{(8.5\times10^{-4})(1)^2} \\ &+ \overset{Sr^{2+}}{(1.6\times10^{-4})(2)^2} + \overset{BO_3^{3-}}{(5\times10^{-4})(3)^2}] = 0.772\,\mathrm{M} \end{aligned} \quad (1)$$

2.2. Sample characterization

The crystals deposited on the surfaces of UHMWPE coupons were imaged by scanning electron microscopy (SEM, Zeiss-Neon 40 EsB, 10 kV), after sputter coating with a 10 nm-thick layer of Au–Pd alloy prior to imaging. The phase composition of the deposited crystals (upon scraping those away from the surfaces of coupons) was investigated by Cu Kα X-ray diffraction using a Bruker D8 Advance diffractometer (XRD, 40 kV, 40 mA, 0.02° steps, 8 s at each step, single crystal quartz sample holders). The scraped crystals were ground in an agate mortar prior to XRD runs. Fourier-transform infrared spectroscopy (FTIR, Spectrum One, PerkinElmer) samples of the scraped crystals were prepared by mixing them with spectral-grade KBr powders at the ratio of 1 mg sample-to-300 mg KBr in an agate mortar using an agate pestle. Transparent FTIR pellets with a diameter of 10 mm were pressed in stainless steel dies at 1000 kg applied for 1 min. FTIR data were collected with 128 scans, at 2 cm^{-1} resolution, over the range of 4000–700 cm^{-1}. Quantitative magnesium analyses of the scraped crystals were performed by using inductively-coupled plasma atomic emission spectroscopy (ICP-AES, Model 61E, Thermo Electron). For the ICP-AES analyses, 70 mg portions of powder samples were dissolved in 5 mL of concentrated HNO_3 solution. The wettability of non-coated and aragonite-coated UHMWPE coupons were determined by using a computer-controlled contact angle goniometer (*Theta Lite*, Biolin Scientific, Espoo, Finland) *via* the static sessile drop method (3 μL drop volume) with deionized water at RT. The photographs captured by the goniometer's camera were analyzed by using the software ImageJ (National Institutes of Health) to measure the contact angle (θ). The reported contact angles were the average of six measurements on each sample.

3. Results and discussion

UHMWPE substrates were preferred in this study, instead of, *e.g.*, ordinary glass slides, to eliminate any issue(s) of the undesired leaching of inorganic ions from the substrate itself to interact with the crystallization and coating process. Artificial seawater (ASW) of Table 1, being a HCO_3^--deficient solution, did not form any crystals on the surfaces of UHMWPE coupons even after 20 days of immersion at 30 °C. The HCO_3^-/Ca^{2+} molar ratio of ASW is only 0.273, which is rather low for extensive $CaCO_3$ nucleation to occur. To increase the HCO_3^-/Ca^{2+} molar ratio in the ACS-1, ACS-2 and ACS-3 solutions to 1.75, the amounts (in g) of $NaHCO_3$ and $CaCl_2{\cdot}2H_2O$ was made equal to one another. The amounts of both $NaHCO_3$ and $CaCl_2{\cdot}2H_2O$ used in preparing the ACS-2 and ACS-3 solutions were respectively increased by 83 and 166% in comparison to those of the ACS-1 solution. ACS-1, ACS-2 and ACS-3 solutions of Table 1 were

Table 1
Recipes of ASW [35] and ACS solutions (volume basis: 500 mL).

Salt	ASW		ACS-1		ACS-2		ACS-3		ACS-4		ACS-5	
	(mM)	(g)	(mM)	(g)	(mM)	(g)	(mM)	(g)	(mM)	(g)	(mM)	(g)
NaCl	420	12.273	420	12.273	420	12.273	420	12.273	420	12.273	–	–
$MgCl_2 \cdot 6H_2O$	54.60	5.550	54.60	5.550	54.60	5.550	54.60	5.550	54.60	5.550	54.60	5.550
Na_2SO_4	28.80	2.045	28.80	2.045	28.80	2.045	28.80	2.045	28.80	2.045	–	–
$CaCl_2 \cdot 2H_2O$	10.23	0.752	10.23	0.752	18.72	1.376	27.21	2.000	10.23	0.752	10.23	0.752
KCl	9.30	0.347	9.30	0.347	9.30	0.347	9.30	0.347	9.30	0.347	–	–
$NaHCO_3$	2.79	0.117	17.93	0.752	32.81	1.376	47.69	2.000	104.92	4.400	104.92	4.400
KBr	0.85	0.051	0.85	0.051	0.85	0.051	0.85	0.051	0.85	0.051	–	–
H_3BO_3	0.50	0.016	0.50	0.016	0.50	0.016	0.50	0.016	0.50	0.016	–	–
$SrCl_2 \cdot 6H_2O$	0.16	0.021	0.16	0.021	0.16	0.021	0.16	0.021	0.16	0.021	–	–
NaF	0.07	0.0015	0.07	0.0015	0.07	0.0015	0.07	0.0015	0.07	0.0015	–	–
Ionic strength	0.717 M		0.732		0.772		0.813		0.819		0.294	

designed to have the constant HCO_3^-/Ca^{2+} molar ratio of 1.75. This made it possible to observe the influence of increased concentration of Ca^{2+} and HCO_3^- ions at a constant HCO_3^-/Ca^{2+} molar ratio, constant temperature and at constant nucleation/coating time through the ACS-1, ACS-2 and ACS-3 solutions. ACS-4 and ACS-5 solutions will be discussed later.

The XRD data of Fig. 1a showed the formation of aragonite, as the major phase, on all UHMWPE coupons soaked at 30 °C in the ACS-1, ACS-2 and ACS-3 solutions for 48 h. While the ACS-1 and ACS-2 solutions produced single-phase aragonite crystals (conforming to the crystallographic reflections listed in the ICDD PDF 41-1475 card), the aragonite crystals formed in the ACS-3 solution were found to be contaminated with about 10–15% magnesian-calcite (R-*3c* (167), ICDD PDF 43-0697).

The formation of crystals in the ACS-1 through three solutions was not immediate, it was followed by an incubation period of 4 h during which the solutions remained optically transparent. This observation surely does not exclude the possibility of the presence of invisible nanoclusters of either amorphous (ACC, amorphous calcium carbonate [49]) or nanocrystalline calcium carbonate. The presence or absence of such nanoclusters (which would not be visible to the naked eye) needs to be further confirmed by using dynamic light scattering techniques. Synthetic body fluid (SBF) solutions, for instance, which deposit cryptocrystalline or amorphous calcium phosphate on immersed substrates, contain such nanoclusters although the freshly-prepared SBFs remain optically transparent [50]. The FTIR data of crystals deposited on the UHMWPE coupons in solutions ACS-1, ACS-2 and ACS-3 are given in Fig. 1b. The IR bands observed at 1798–1570 ($\nu_1 + \nu_4$ overtones and combinations bands), 1481 (ν_3 anti-symmetric stretching mode), 1083 (ν_1 symmetric stretching mode), 855-841 (ν_2 out-of-plane bending mode) and 714–702 cm^{-1} (ν_4 in-plane bending mode) corresponded to those of aragonite [51].

The results of ICP-AES analyses of crystals formed at 30 °C on UHMWPE substrates (in 48 h) in ACS-1, ACS-2 and ACS-3 solutions consistently gave a magnesium content of 0.35 ± 0.02 wt% ($n = 3$), with a mean value of 0.357 wt% (3570 ppm). Since the Mg^{2+}/Ca^{2+} molar ratios of ACS-1, ACS-2 and ACS-3 solutions were all at or above 2.00, the constant Mg wt% registered in the samples meant that to find smaller percentages of Mg in the formed crystals the above molar ratio should be smaller. Koga and Nishikawa [52] reported the presence of 4200 ppm magnesium in biogenic coral aragonite, which is formed in natural seawater over an extended period of time.

Artificial seawater (ASW), similar to natural seawater, has a high Mg^{2+}/Ca^{2+} molar ratio of 5.34, which is identical with that of the ACS-1 solution of Table 1. However, the ACS-2 and ACS-3 solutions of Table 1 were so designed that this molar ratio would drop to 2.92 and 2.00, respectively. Reddy and Nancollas [53] predicted that in distilled water, free of NaCl and KCl, when Mg^{2+} and Ca^{2+} ions are made equimolar, the major phase would be aragonite instead of magnesian (calcite).

Simkiss [54], on the other hand, found that in a solution containing only NaCl (26.98 g/L), $MgCl_2 \cdot 6H_2O$ (10.91 g/L), $CaCl_2$ (1.13 g/L), and $NaHCO_3$ (0.6 g/L) single-phase aragonite will precipitate instead of calcite. The solution of Simkiss [54], although it was not a complete ASW [33–35], had the Mg^{2+}/Ca^{2+} molar ratio of 5.3 and the findings of Simkiss [54] and the data presented in Fig. 4 of the report of Choudens-Sanchez and Gonzalez [55] were in strong support of the single-phase aragonite observed in the ACS-1 and ACS-2 solutions of this study. The data presented in Fig. 1 of the report of Bots et al. [56], which examined the combined influence of SO_4^{2-} concentration and Mg^{2+}/Ca^{2+} molar ratio of seawater on the $CaCO_3$ polymorphism, also supported the single-phase aragonite formation in the ACS-1 and ACS-2 solutions of this study.

Magnesian-calcite [57], having XRD d-spacings (ICDD PDF 43-0697) noticeably different than those of pure calcite (ICDD PDF 5-0586), crystallization in seawater is greatly hindered by Mg^{2+} in favor of aragonite, when it is present at a high proportion to Ca^{2+} as in seawater [18,58]. The long incubation time (4 h) observed for the ACS-1, ACS-2 and ACS-3 solutions is also caused by this high Mg^{2+}/Ca^{2+} ratio, which partially delayed the nucleation as well. The reason for that partial nucleation inhibition is the thermodynamic difficulty in forming crystalline and anhydrous magnesite ($MgCO_3$) in aqueous solutions, in lieu of monoclinic hydromagnesite ($Mg_5(CO_3)_4(OH)_2 \cdot 4H_2O$)-like phases, at temperatures less than 100 °C and at pCO_2 less than 50 atm [59]. Mg^{2+} ions form strong solvation shells in aqueous solutions. Pavlov et al. [60] computed the binding energy of water molecules to Mg^{2+} in the aqueous $[Mg(H_2O)_n](H_2O)_m{}^{2+}$ clusters to be significantly higher than to Ca^{2+} in $[Ca(H_2O)_n](H_2O)_m{}^{2+}$. However, ASW or ACS solutions would probably not contain such pure Mg or Ca clusters; the clusters in ASW or ACS should simultaneously contain Mg and Ca. The literature lacks any experimental or computational data on the $[(Mg, Ca)(H_2O)_n](H_2O)_m{}^{2+}$ clusters of ASW or ACS solutions. In such bi-metallic clusters, the availability of Ca^{2+} for aragonite or magnesian-calcite formation is expected to be hindered by the presence of Mg^{2+}, which helps to explain the long incubation times observed in this study for aragonite nucleation. The aragonite precipitation in distilled water (free of Mg^{2+} and other ions of ASW) are known not to display such long incubation times [21–32].

At the end of all experiments, aggregates of feather-like solids were also observed to float on the liquid–gas surface of ACS-1 through ACS-3 solutions of Table 1. Such white aggregates were carefully collected and analyzed by XRD to find that they were comprised of single-phase aragonite. ACS solutions of Table 1 contain much higher amounts of dissolved $NaHCO_3$ than that present in ASW [33–35]. Eqs. (2a) and (2b) describe the production of CO_2 (g) in bicarbonate-dominated solutions such as ACS. The removal of CO_2 (g) from the ACS solutions, favored by an increase in solution

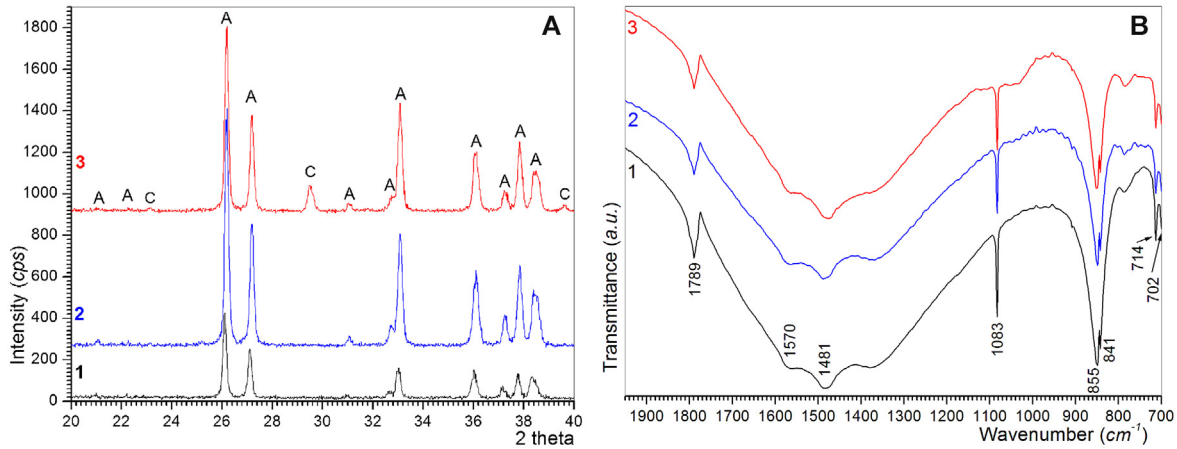

Fig. 1. (a) XRD traces of autogenously formed spherules in ACS-1, ACS-2 and ACS-3 solutions at 30 °C in 48 h (A: aragonite, C: magnesian-calcite peaks; numbers in color denote the solutions, from Table 1). (b) FTIR spectra of autogenously formed spherules in ACS-1, ACS-2 and ACS-3 solutions at 30 °C in 48 h (numbers in color on the left denote the solutions, from Table 1). (For interpretation of the references to color in this figure legend, the reader is referred to the web version of this article.)

temperature from the ambient to 30 °C, results in a local increase in the solution pH at the liquid–gas interface, as indicated by Eq. (2b) [61]. Therefore, the liquid–gas interface of ACS solutions, subject to a pH increase, became a preferential site for aragonite crystallization. The reversible reaction of Eq. (2c) (also with Eq. (2b))

$$NaHCO_3(s) = Na^+(aq) + HCO_3^-(aq) \quad (2a)$$

$$HCO_3^-(aq) = OH^-(aq) + CO_2(g) \quad (2b)$$

$$CO_2(g) + H_2O = H^+(aq) + HCO_3^-(aq). \quad (2c)$$

summarizes the pCO_2-dependent mechanism of aragonite dissolution-reprecipitation processes taking place in coral reefs [31,62–66] as a result of ocean acidification caused by the increase in atmospheric CO_2(g) content. The ACS solutions sealed in air-tight HDPE bottles of this study, therefore, utilized the HCO_3^- (aq)-CO_2 (g) pair as the weak pH buffering agent, just like the human blood having a HCO_3^- concentration of 27 mM does.

The SEM photomicrographs of Fig. 2 show the deposition of aragonite onto UHMWPE coupons soaked in ACS-1, ACS-2 and ACS-3 solutions at 30 °C for 48 h. The decrease in the Mg^{2+}/Ca^{2+} molar ratios of solutions (*i.e.*, ACS-1 sol: 5.34, ACS-2 sol: 2.92 and ACS-3 sol: 2.00) with a simultaneous increase in the Ca^{2+} and HCO_3^- concentrations, had quite a strong influence on the extent of surface coverage. While the percentage coverage of the available surface in the ACS-1 solution (Fig. 2a) with aragonite crystals was significantly low, it first increased to around 45% coverage in the ACS-2 solution (Fig. 2c) and then to 100% in the ACS-3 solution (Fig. 2e). The insets in Fig. 2a, c and e showed the morphology of aragonite spherules at higher magnifications.

When such solutions could find use in depositing crystalline aragonite on the surfaces of other porous or non-porous biomaterials, the percentage of surface coverage to be achieved with a specific solution becomes a significant issue for the deposition engineer to consider. This study, therefore, showed for the first time that in order to completely cover the surface of an UHMWPE coupon with the major phase of aragonite at 30 °C and in 48 h, the solution (ACS-3) should have a Mg^{2+}/Ca^{2+} molar ratio slightly higher than 2, and [Ca^{2+}] and [HCO_3^-] concentrations of about 27.2 mM and 47.7 mM, respectively.

The high-magnification images provided in Fig. 2b, d and f, and their insets, for solutions ACS-1, ACS-2 and ACS-3, respectively, indicated an interesting phenomenon which was not mentioned frequently in the aragonite synthesis literature. The aragonite particles formed in ACS-1 solution (Fig. 2b and its inset) seemed to contain poorly-defined or immature crystal facets, in comparison to those well-described facets shown in Fig. 2f (and its inset). The passage from the micro-morphology of the particles of Fig. 2b (ACS-1) to those of Fig. 2f (ACS-3) is accompanied with an increase in solution [Ca^{2+}] and [HCO_3^-] concentrations and a simultaneous decrease in the Mg^{2+}/Ca^{2+} molar ratios of solutions. This phenomenon may be reminiscent of a maturation process taking place at the nano-scale.

The macro- and micro-morphology of $CaCO_3$ nucleating in a Ca^{2+} and HCO_3^--containing solution strongly depends on its actual HCO_3^-/Ca^{2+} ratio. Another biomimicking ACS solution of this study, *i.e.*, ACS-4 of Table 1, with a HCO_3^-/Ca^{2+} molar ratio of 10.24, formed ooids of single-phase aragonite on UHMWPE coupons upon only heating the ACS-4 at 30 °C for 48 h (Fig. 3a). A monolayer of aragonite ooids covered the edges of coupons uniformly (Fig. 3a and b). These aragonite ooids (100–200 μm in diameter) were comprised of the mortar-and-brick-type stacking of 200–300 nm-thick (inset of Fig. 3a) crystals. The XRD data of ACS-4 deposits indicated single-phase aragonite (Fig. 3c).

Wettability of non-coated (*i.e.*, pristine) UHMWPE and aragonite-coated samples were studied *via* contact angle goniometry with deionized water at room temperature. Fig. 4a shows the hydrophobic nature of pristine UHMWPE samples. The contact angle (θ) of pristine UHMWPE was found to be 80°, which is confirming the hydrophobic character of UHMWPE reported previously by Deng et al. [67] and Riveiro et al. [68]. The contact angle of ACS-2-coated sample surfaces, previously shown in Fig. 2c, was around 22° (Fig. 4b), whereas that of the ACS-3-coated sample of Fig. 2e (Fig. 4c) was found to be less than 10°. The contact angle of ACS-4-coated sample surfaces, previously shown in Fig. 3a, was around 15° (Fig. 4d). ACS solutions of this study are, therefore, effective in changing the hydrophobic surfaces of UHMWPE samples to hydrophilic. Any increase in the wettability of UHMWPE, as shown in this study by aragonite deposition, may further enhance the adsorption of blood plasma proteins [69] to the surfaces of such clinically implantable materials.

The ACS-5 solution of Table 1, which does not contain NaCl, KCl, *etc.* and does suffer from having a lower ionic strength in comparison to the ACS-1 through ACS-4 solutions, cannot be named as truly biomimicking since it does not possess the salinity of (35 parts per thousand) of seawater; however, it answers the following question. Is it possible to achieve a similar crystallization behavior with a simpler solution (ACS-5) stripped of all other inorganic ingredients except $MgCl_2{\cdot}6H_2O$, $CaCl_2{\cdot}2H_2O$ and $NaHCO_3$? The answer was positive (Fig. 3b). The ACS-5 solution resulted in, after only 3 min of an incubation period, similar aragonite ooids with the same

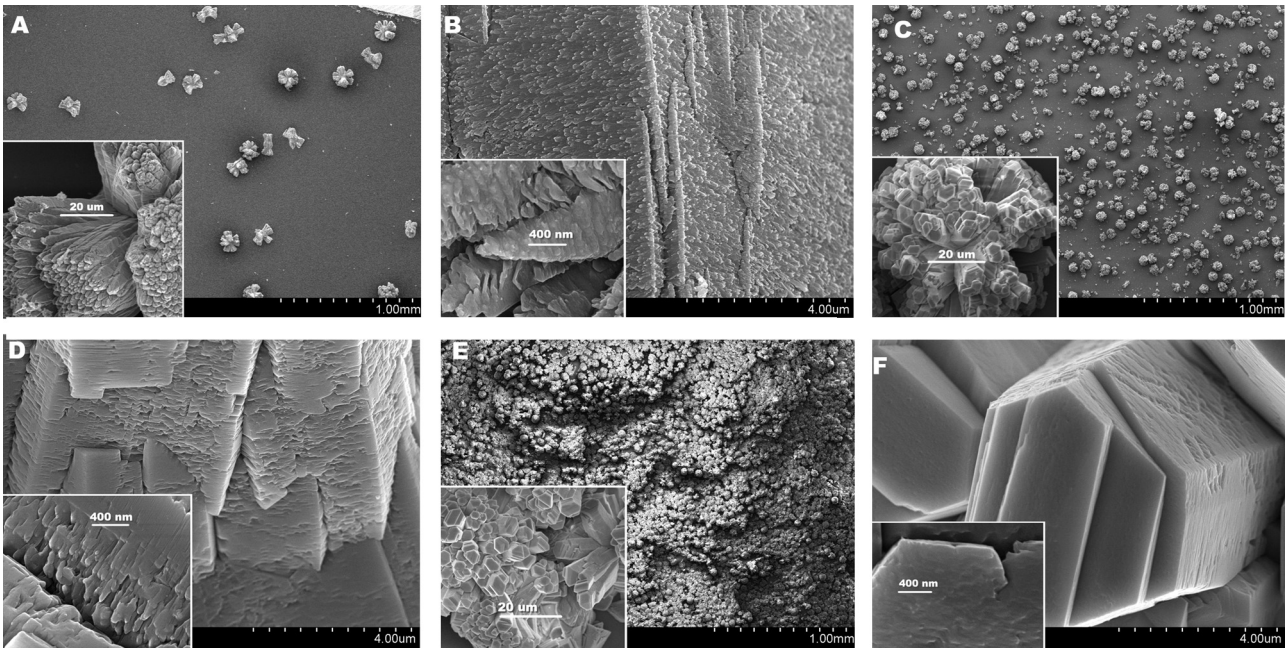

Fig. 2. SEM photomicrographs of aragonite spherules deposited on the surfaces of UHMWPE coupons, in 48 h at 30 °C, in ACS-1 solutions (a) and (b); ACS-2 solutions (c) and (d); ACS-3 solutions (e) and (f).

dimensions as those of biomimicking ACS-4. Nevertheless, the XRD data (Fig. 3c) of ACS-4 and ACS-5 deposits were different. The ACS-5 deposits contained magnesian-calcite (ICDD PDF 43-0697), whose (1 0 4) crystallographic reflection is shifted to 29.71° 2θ instead of 29.41° of calcite (ICDD PDF 5-0586) for the same reflection. The incorporation of Mg^{2+} ion of smaller radius (86 pm), in comparison to larger Ca^{2+} (114 pm), into the calcite lattice also shows itself in slightly reduced lattice parameters for the magnesian-calcite.

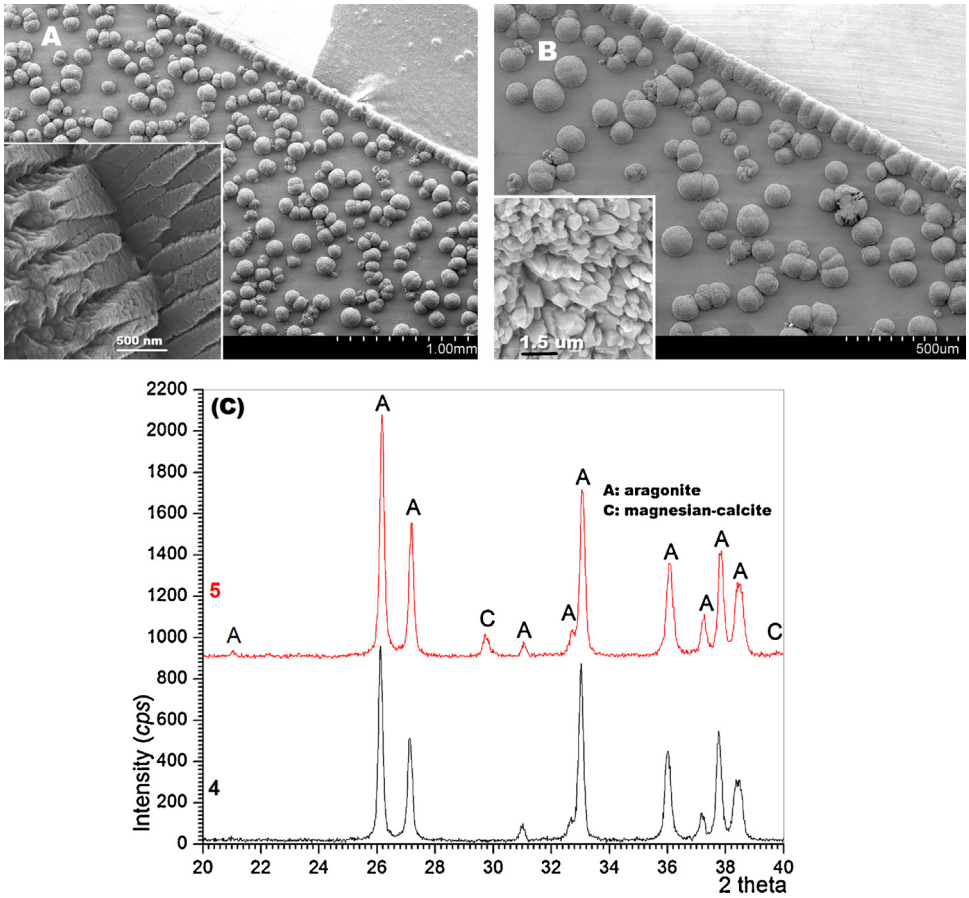

Fig. 3. SEM photomicrographs of aragonite ooids deposited, at 30 °C in 48 h, on the surfaces of UHMWPE coupons (a) in ACS-4 solutions, (b) in ACS-5 solutions, and (c) XRD traces of deposits obtained in ACS-4 and ACS-5 solutions.

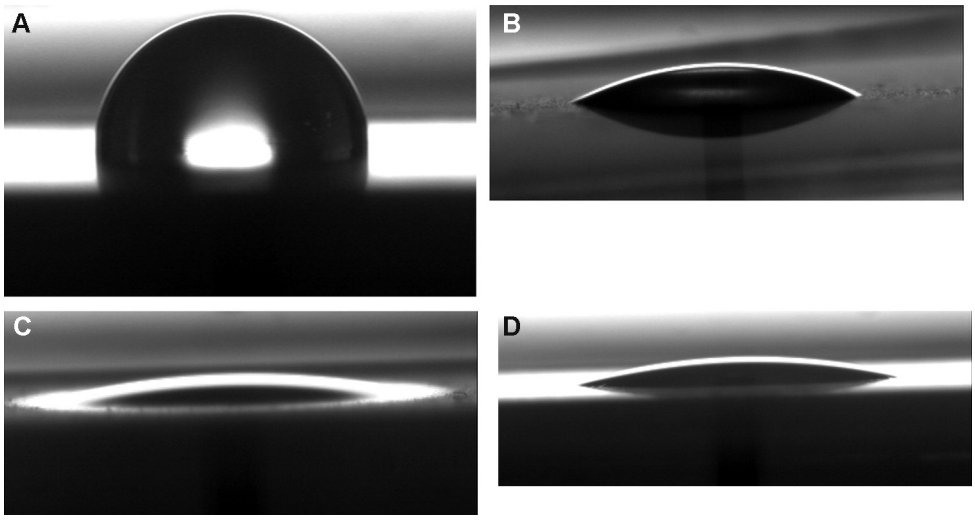

Fig. 4. Contact angle goniometry photographs captured on (a) non-coated UHMWPE coupon, (b) ACS-2-coated sample of Fig. 2c, (c) ACS-3-coated sample of Fig. 2e, (d) ACS-4-coated sample of Fig. 3a. The contact angles reported in the manuscript were determined 10 s after the drop touched the samples.

Magnesian-calcite is the phase of micro-porous skeletons of sea stars (*i.e.*, starfish) [70].

The ACS-3 solution (Table 1) exhibited full coverage of the available surfaces of UHMWPE coupons with a biphasic mixture of aragonite (85–90%) and magnesian-calcite (10–15%) in 48 h at 30 °C. That solution employed the highest concentrations of Ca^{2+} and HCO_3^- ions in this study. The following question needs to be answered. Would the reaction of 4 g/L $CaCl_2{\cdot}2H_2O$ and 4 g/L $NaHCO_3$ (see Table 1) at a HCO_3^-/Ca^{2+} molar ratio of 1.75 in deionized water, instead of ASW, necessarily produce calcite? The negative answer to this question was provided by the XRD, FTIR and SEM data of Fig. 5.

Upon slowly adding (the first 12.5 mL portion being added in 3 min, drop-by-drop, followed by adding the remaining 237.5 mL in 50 s) 250 mL of deionized water having 4.00 g $CaCl_2{\cdot}2H_2O$ dissolved in it to 750 mL of deionized water with 4.00 g of $NaHCO_3$ under vigorous stirring, one obtains single-phase vaterite (ICDD PDF 33-0268) as shown in Fig. 5a. One needs to note the absence

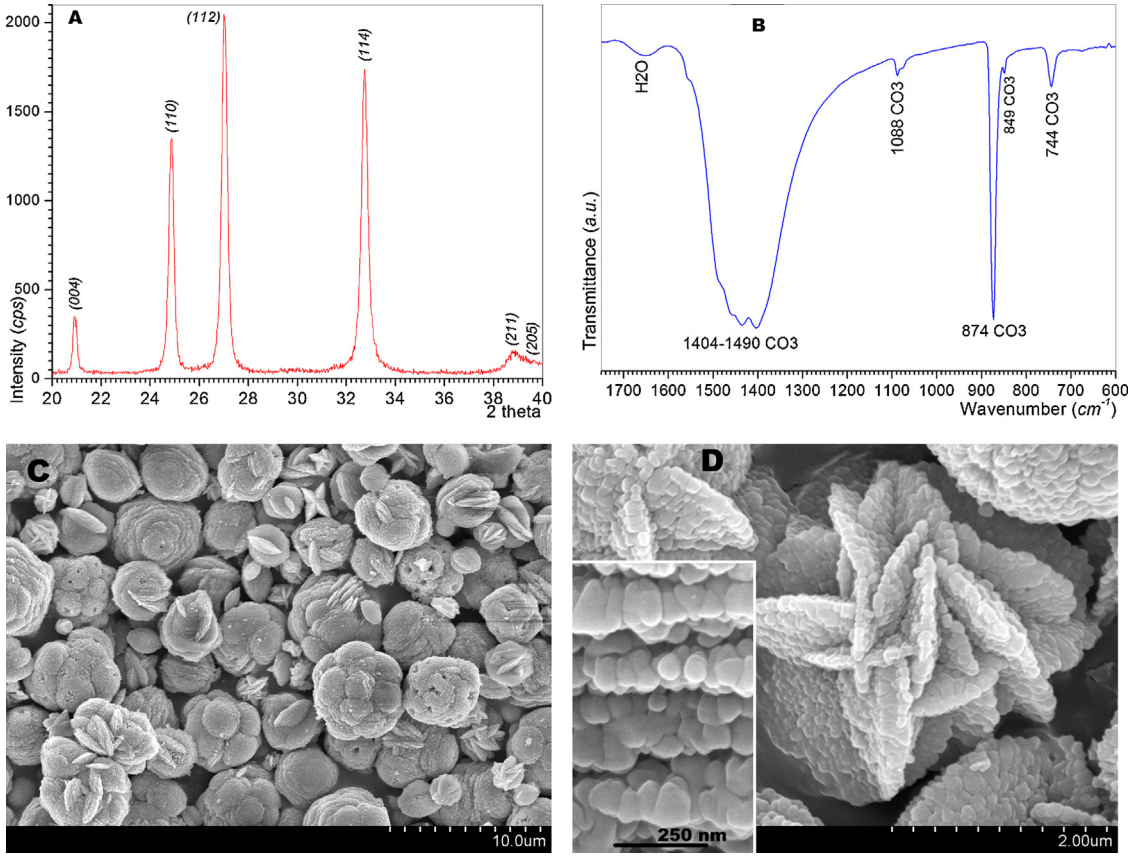

Fig. 5. (a) XRD, (b) FTIR, (c) and (d) SEM photomicrographs of vaterite powders obtained when the Ca-chloride dihydrate (4 g/L) and Na-bicarbonate (4 g/L) of ACS-3 solution were reacted at RT in deionized water, followed by immediate filtering of suspensions.

of the characteristic 713 cm^{-1} IR band of calcite in Fig. 5b. It is usually difficult to synthesize vaterite powders, in the absence of any organic molecules, without the (1 0 4) peak of calcite being visible in their XRD traces [71,72]. The SEM photomicrographs of Fig. 5c and d showed that the vaterite particles comprised of 100 nm nanoparticles.

The above experimental finding denotes that the ACS-1, ACS-2 and ACS-3 solutions of Table 1, which all employed equal weights of $CaCl_2{\cdot}2H_2O$ and $NaHCO_3$, would not be prone to form only calcite if their Ca-chloride dihydrate and Na-bicarbonate salts were reacted with one another in deionized water at RT in lieu of artificial seawater. The disc-like (or pumpkin-like) vaterite particles shown in Fig. 5c and d were first reported in 1897 by Vater [6] himself in the form of hand-drawn sketches.

The preferred morphology of a crystal (whether it is calcite, vaterite or aragonite) is usually determined by the surface energy and the related growth rate of various crystallographic planes. Calcite crystals which exhibit rhombohedral geometry (with a theoretical density of 2.711 g/cm^3) almost always expose their hydrated (1 0 4) planes of lowest free energy, which are oxygen terminated surface planes [73,74]. Vaterite (2.665 g/cm^3) and aragonite (2.927 g/cm^3) crystals, on the other hand, typically present their low surface free energy (0 1 0) planes and both of these (0 1 0) vaterite and aragonite planes are Ca terminated planes. Interestingly, all other possible surface planes of vaterite and aragonite are also Ca terminated planes [74].

Aragonite is recently shown to be able to rapidly respond to SBF solutions (at the human body temperature of 37 °C) by transforming itself into bone mineral-like carbonated apatitic calcium phosphate, while calcite does not have this ability [75]. $CaCO_3$ is much more resorbable than β-tricalcium phosphate (β-$Ca_3(PO_4)_2$) and this fact was proved by the *in vitro* cell culture study of Monchau et al. [76], which directly compared Ca-hydroxyapatite, β-tricalcium phosphate, and $CaCO_3$ with one another by using both human and rat osteoclasts.

To summarize, while the biomimicking ACS-1 and ACS-2 (HCO_3^-/Ca^{2+} ratio of 1.75) solutions were able to deposit (high magnification insets of Fig. 2) "botryoidal" [77] splays of radial-fibrous single-phase aragonite at 30 °C (in 48 h), the ACS-4 (HCO_3^-/Ca^{2+} ratio of 10.2) solution of this study showed the formation of single-phase aragonite ooids having a mortar-and-brick-type nanostructure (inset of Fig. 3a). This study performed with entirely inorganic artificial seawater-like solutions at 30 °C may be helpful to research which try to understand and duplicate the mortar-and-brick-type [78,79] nanostructure of mollusc bivalve shells or nacre of mother-of-pearl in the presence of organic molecules/matter.

4. Conclusions

Entirely inorganic, five different aragonite coating solutions (ACS) were developed, for the first time, and used to deposit aragonite on UHMWPE coupons kept undisturbed in these solutions for 48 h at 30 °C. The ACS solutions were inspired by the artificial seawater (ASW). The temperature chosen (30 °C) for solution treatments mimicked that of the tropical sea surface.

The ACS solutions were initially free of any visible precipitates and started to slowly form a monolayer of aragonite spherules only upon heating to 30 °C, after an incubation period of 4 h at the temperature. ACS solutions might be useful in producing various aragonite-biomaterial hybrids. Two of the ACS solutions, significantly enriched with calcium and bicarbonate ions with respect to those present in the formulation of ASW, deposited biphasic aragonite-magnesian calcite. A robust and totally inorganic process for calcite-free vaterite synthesis was reported. This process used the same bicarbonate ion concentration with two of the ACS solutions.

5. Notes

Certain commercial equipments or instruments are only identified in this article to foster understanding. Such identification does not imply recommendation or endorsement by the author, nor does it imply that the equipments identified are necessarily the best available for the purpose.

Acknowledgment

This study was conceived and performed in the Department of Biomedical Engineering of Yeditepe University, Istanbul, Turkey, while the author was a full professor there between 2006 and 2010. The aforesaid department does not have a graduate program and is designed for undergraduate education only.

References

[1] S. Mann, Biomineralization: Principles and Concepts in Bioinorganic Materials Chemistry, Oxford University Press, Oxford, 2001.
[2] V.C. Allison, The growth of stalagmites and stalactites, J. Geol. 31 (1923) 106–125.
[3] C.M. Sherwin, J.U.L. Baldini, Cave air and hydrological controls on prior calcite precipitation and stalagmite growth rates: implications for palaeoclimate reconstructions using speleothems, Geochim. Cosmochim. Acta 75 (2011) 3915–3929.
[4] Y. Kojima, A. Kawanobe, T. Yasue, Y. Arai, Synthesis of amorphous calcium carbonate and its crystallization, J. Ceram. Soc. Jpn. 101 (1993) 1145–1152.
[5] L. Brecevic, D. Kralj, On calcium carbonates: from fundamental research to application, Croat. Chem. Acta 80 (2007) 467–484.
[6] H. Vater, Ueber den einfluss der loesungsgenossen auf die krystallisation des calciumcarbonates, Z. Kristallogr. Mineral. 27 (1897) 477–512.
[7] L.N. Plummer, E. Busenberg, The solubilities of calcite, aragonite and vaterite in CO_2–H_2O solutions between 0 and 90 °C, and an evaluation of the aqueous model for the system $CaCO_3$–CO_2–H_2O, Geochim. Cosmochim. Acta 46 (1982) 1011–1040.
[8] G.H. Rau, CO_2 mitigation via capture and chemical conversion in seawater, Environ. Sci. Technol. 45 (2011) 1088–1092.
[9] S. Zhong, A. Mucci, Partitioning of rare earth elements (REEs) between calcite and seawater solutions at 25 °C and 1 atm, and high dissolved REE concentrations, Geochim. Cosmochim. Acta 59 (1995) 443–453.
[10] P. Zuddas, A. Mucci, Kinetics of calcite precipitation from seawater: I. A classical chemical kinetics description for strong electrolyte solutions, Geochim. Cosmochim. Acta 58 (1994) 4353–4362.
[11] P. Zuddas, A. Mucci, Kinetics of calcite precipitation from seawater: II. The influence of the ionic strength, Geochim. Cosmochim. Acta 62 (1998) 757–766.
[12] S. Zhong, A. Mucci, Calcite and aragonite precipitation from seawater solutions of various salinities: precipitation rates and overgrowth compositions, Chem. Geol. 78 (1989) 283–299.
[13] A. Mucci, R. Canuel, S. Zhong, The solubility of calcite and aragonite in sulfate-free seawater and the seeded growth kinetics and composition of the precipitates at 25 °C, Chem. Geol. 74 (1989) 309–320.
[14] A. Mucci, Influence of temperature on the composition of magnesian calcite overgrowths precipitated from seawater, Geochim. Cosmochim. Acta 51 (1987) 1977–1984.
[15] A. Mucci, J.W. Morse, The solubility of calcite in seawater solutions of various magnesium concentration, I_t = 0.697 m at 25 °C and one atmosphere total pressure, Geochim. Cosmochim. Acta 48 (1984) 815–822.
[16] A. Mucci, J.W. Morse, The incorporation of Mg^{2+} and Sr^{2+} into calcite overgrowths: Influences of growth rate and solution composition, Geochim. Cosmochim. Acta 47 (1983) 217–233.
[17] J.W. Morse, A. Mucci, F.J. Millero, The solubility of calcite and aragonite in seawater of 35% salinity at 25 °C and atmospheric pressure, Geochim. Cosmochim. Acta 44 (1980) 85–94.
[18] R.A. Berner, The role of magnesium in the crystal growth of calcite and aragonite from sea water, Geochim. Cosmochim. Acta 39 (1975) 489–504.
[19] R.A. Berner, Activity coefficients of bicarbonate, carbonate and calcium ions in sea water, Geochim. Cosmochim. Acta 29 (1965) 947–965.
[20] R.A. Berner, P. Wilde, Dissolution kinetics of calcium carbonate in sea water: I. Saturation state parameters for kinetic calculations, Am. J. Sci. 272 (1972) 826–839.
[21] W.L. Bragg, The structure of aragonite, P. R. Soc. Lond. A-Conta 105 (1924) 16–39.
[22] H.L.J. Backstrom, The thermodynamic properties of calcite and aragonite, J. Am. Chem. Soc. 47 (1925) 2432–2442.

[23] J.L. Wray, F. Daniels, Precipitation of calcite and aragonite, J. Am. Chem. Soc. 79 (1957) 2031–2034.
[24] P.M. Bills, The precipitation of calcium carbonate polymorphs *in vitro* at 37 °C, Calcif. Tissue Int. 37 (1985) 174–177.
[25] Y. Ota, S. Inui, T. Iwashita, T. Kasuga, Y. Abe, Preparation of aragonite whiskers, J. Am. Ceram. Soc. 78 (1995) 1983–1984.
[26] L. Wang, I. Sondi, E. Matijevic, Preparation of uniform needle-like aragonite particles by homogeneous precipitation, J. Colloid Interface Sci. 218 (1999) 545–553.
[27] J.W. Ahn, K.S. Choi, S.H. Yoon, H. Kim, Synthesis of aragonite by the carbonation process, J. Am. Ceram. Soc. 87 (2004) 286–288.
[28] S. Thachepan, M. Li, S.A. Davis, S. Mann, Additive-mediated crystallization of complex calcium carbonate superstructures in reverse microemulsions, Chem. Mater. 18 (2006) 3557-3361.
[29] W.K. Park, S.J. Ko, S.W. Lee, K.H. Cho, J.W. Ahn, C. Han, Effects of magnesium chloride and organic additives on the synthesis of aragonite precipitated calcium carbonate, J. Cryst. Growth 310 (2008) 2593–2601.
[30] R. Beck, J.P. Andreassen, The onset of spherulitic growth in crystallization of calcium carbonate, J. Cryst. Growth 312 (2010) 2226–2238.
[31] K.K. Sand, J.D. Rodriguez-Blanco, E. Makovicky, L.G. Benning, S.L.S. Stipp, Crystallization of $CaCO_3$ in water-alcohol mixtures: spherulitic growth, polymorph stabilization, and morphology change, Cryst. Growth Des. 12 (2012) 842–853.
[32] J. Jiang, J. Ye, G. Zhang, X. Gong, L. Nie, J. Liu, Polymorph and morphology control of $CaCO_3$ via temperature and PEG during the decomposition of $Ca(HCO_3)_2$, J. Am. Ceram. Soc. 95 (2012) 3735–3738.
[33] D.R. Kester, I.W. Duedall, D.N. Connors, R.M. Pytkowicz, Preparation of artificial seawater, Limnol. Oceanogr. 12 (1967) 176–179.
[34] J. Lyman, R.H. Fleming, Composition of sea water, J. Mar. Res. 3 (1940) 134–146.
[35] ASTM Standard D1141-98, Standard Practice for the Preparation of Substitute Ocean Water, American Society for Testing and Materials (ASTM), West Conshohocken, PA, USA, 2013.
[36] M.D. Patey, M.J.A. Rijkenberg, P.J. Statham, M.C. Stinchcombe, E.P. Achterberg, M. Mowlem, Determination of nitrate and phosphate in seawater at nanomolar concentrations, Trends Anal. Chem. 27 (2008) 169–182.
[37] Ch Barchiche, C. Deslouis, D. Festy, O. Gil, Ph. Refait, S. Touzain, B. Tribollet, Characterization of calcareous deposits in artificial seawater by impedance techniques 3 – deposit of $CaCO_3$ in the presence of Mg(II), Electrochim. Acta 48 (2003) 1645–1654.
[38] Ch. Barchiche, C. Deslouis, O. Gil, S. Joiret, Ph. Refait, B. Tribollet, Role of sulphate ions on the formation of calcareous deposits on steel in artificial seawater: the formation of green rust compounds during cathodic protection, Electrochim. Acta 54 (2009) 3580–3588.
[39] H. Moeller, The influence of Mg^{2+} on the formation of calcareous deposits on a freely corroding low carbon steel in seawater, Corros. Sci. 49 (2007) 1992–2001.
[40] H. Karoui, B. Riffault, M. Jeannin, A. Kahoul, O. Gil, M.B. Amor, M.M. Tlili, Electrochemical scaling of stainless steel in artificial seawater: role of experimental conditions on $CaCO_3$ and $Mg(OH)_2$ formation, Desalination 311 (2013) 234–240.
[41] A. Benedetti, L. Magagnin, F. Passaretti, E. Chelossi, M. Faimali, G. Montesperelli, Cathodic protection of carbon steel in natural seawater: effect of sunlight radiation, Electrochim. Acta 54 (2009) 6472–6478.
[42] E. Lee, Y. Noh, N. Hirose, A new method to produce sea surface temperature using satellite data assimilation into an atmosphere-ocean mixed layer coupled model, J. Atmos. Ocean. Technol. 30 (2013) 2926–2943.
[43] J. Segschneider, J. Bentsen, Temperature-dependent remineralization in a warming ocean increases surface pCO_2 through changes in marine ecosystem composition, Glob. Biogeochem. Cycles 27 (2013) 1214–1225.
[44] Y. Abe, T. Kokubo, T. Yamamuro, Apatite coating on ceramics, metals and polymers using a biomimetic process, J. Mater. Sci. Mater. Med. 1 (1990) 233–238.
[45] Bayraktar, A.C. Tas, Chemical preparation of carbonated calcium hydroxyapatite powders at 37 °C in urea-containing synthetic body fluids, J. Eur. Ceram. Soc. 19 (1999) 2573–2579.
[46] A.C. Tas, Submicron spheres of amorphous calcium phosphate forming in a stirred SBF solution at 55 °C, J. Non-Cryst. Solids 400 (2014) 27–32.
[47] H. Pan, X. Zhao, B.W. Darvell, W.W. Lu, Apatite-formation ability – predictor of bioactivity? Acta Biomater. 6 (2010) 4181–4188.
[48] P. Debye, E. Huckel, The theory of electrolytes I. The lowering of the freezing point and related phenomena, Phys. Z. 24 (1923) 185–206.
[49] P. Raiteri, J.D. Gale, Water is the key to nonclassical nucleation of amorphous calcium carbonate, J. Am. Chem. Soc. 132 (2010) 17623–17634.
[50] A. Oyane, K. Onuma, T. Kokubo, A. Ito, Clustering of calcium phosphate in the system $CaCl_2$–H_3PO_4–KCl–H_2O, J. Phys. Chem. B 103 (1999) 8230–8235.
[51] F.Z. Zakaria, J. Mihaly, I. Sajo, R. Katona, L. Hajba, F.A. Aziz, J. Mink, FT-Raman and FTIR spectroscopic characterization of biogenic carbonates from *Philippine venus* seashell and *Porites* sp. coral, J. Raman Spectrosc. 39 (2008) 1204–1209.
[52] N. Koga, K. Nishikawa, Mutual relationship between solid-state aragonite-calcite transformation and thermal dehydration of included water in coral aragonite, Cryst. Growth Des. 14 (2014) 879–887.
[53] M.M. Reddy, G.H. Nancollas, The crystallization of calcium carbonate IV. The effect of magnesium, strontium and sulfate ions, J. Cryst. Growth 35 (1976) 33–38.
[54] K. Simkiss, Variations in the crystalline form of calcium carbonate precipitated from artificial sea water, Nature 201 (1964) 492–493.
[55] V. de Choudens-Sanchez, L.A. Gonzalez, Calcite and aragonite precipitation under controlled instantaneous supersaturation: elucidating the role of $CaCO_3$ saturation state and Mg/Ca ratio on calcium carbonate polymorphism, J. Sediment. Res. 79 (2009) 363–376.
[56] P. Bots, L.G. Benning, R.E.M. Rickaby, S. Shaw, The role of SO_4 in the switch from calcite to aragonite seas, Geology 39 (2011) 331–334.
[57] J.J.M. Lenders, A. Dey, P.H.H. Bomans, J. Spielmann, M.M.R.M. Hendrix, G. de With, F.C. Meldrum, S. Harder, N.A.J.M. Sommerdijk, High-magnesian calcite mesocrystals: a coordination chemistry approach, J. Am. Chem. Soc. 134 (2012) 1367–1373.
[58] L. Fernandez-Diaz, A. Putnis, M. Prieto, C.V. Putnis, The role of magnesium in the crystallization of calcite and aragonite in a porous medium, J. Sediment. Res. 66 (1996) 482–491.
[59] J. Xu, C. Yan, F. Zhang, H. Konishi, H. Xu, H.H. Teng, Testing the cation hydration effect on the crystallization of Ca–Mg–CO_3 systems, Proc. Natl. Acad. Sci. U. S. A. 110 (2013) 17750–17755.
[60] M. Pavlov, P.E.M. Siegbahn, M. Sandstroem, Hydration of beryllium, magnesium, calcium and zinc ions using density functional theory, J. Phys. Chem. A 102 (1998) 219–228.
[61] C.P. Jury, F.I.M. Thomas, M.J. Atkinson, R.J. Toonen, Buffer capacity, ecosystem feedbacks, and seawater chemistry under global change, Water 5 (2013) 1303–1325.
[62] T. McClanahan, The near future of coral reefs, Environ. Conserv. 29 (2002) 460–483.
[63] S. Papadimitriou, H. Kennedy, G. Kattner, G.S. Dieckmann, D.N. Thomas, Experimental evidence for carbonate precipitation and CO_2 degassing during sea ice formation, Geochim. Cosmochim. Acta 68 (2003) 1749–1761.
[64] R. Gangsto, M. Gehlen, B. Schneider, L. Bopp, O. Aumont, F. Joos, Modeling the marine aragonite cycle: changes under rising carbon dioxide and its role in shallow water $CaCO_3$ dissolution, Biogeosciences 5 (2008) 1057–1072.
[65] A. Fransson, M. Chierici, L.A. Miller, G. Carnat, E. Shadwick, H. Thomas, S. Pineault, T.N. Papakyriakou, Impact of sea-ice processes on the carbonate system and ocean acidification at the ice–water interface of the Amundsen gulf, Arctic Ocean, J. Geophys. Res.: Oceans 118 (2013) 7001–7023.
[66] S. Fabre, G. Berger, V. Chavagnac, P. Besson, Origin of cap carbonates: an experimental approach, Palaeogeogr. Palaeocl. 392 (2013) 524–533.
[67] Y. Deng, D. Xiong, S. Shao, Study on biotribological properties of UHMWPE grafted with MPDSAH, Mater. Sci. Eng. C 33 (2013) 1339–1343.
[68] A. Riveiro, R. Soto, J. del Val, R. Comesana, M. Boutinguiza, F. Quintero, F. Lusquinos, J. Pou, Laser surface modification of ultra-high-molecular-weight polyethylene (UHMWPE) for biomedical applications, Appl. Surf. Sci. 302 (2014) 236–242.
[69] L. Vroman, Finding seconds count after contact with blood (and that is all I did), Colloid Surface B 62 (2008) 1–4.
[70] S. Gayathri, R. Lakshmninarayanan, J.C. Weaver, D.E. Morse, R.M. Kini, S. Valiyaveettil, In vitro study of magnesium-calcite biomineralization in the skeletal materials of the seastar *Pisaster giganteus*, Chem. Eur. J. 13 (2007) 3262–3268.
[71] N. Njegic-Dzakula, G. Falini, L. Brecevic, Z. Skoko, D. Kralj, Effects of initial supersaturation on spontaneous precipitation of calcium carbonate in the presence of charged poly-L-amino acids, J Colloid Interface Sci. 343 (2010) 553–563.
[72] G.T. Zhou, Q.Z. Yao, S.Q. Fu, Y.B. Guan, Controlled crystallization of unstable vaterite with distinct morphologies and their polymorphic transition to stable calcite, Eur. J. Mineral. 22 (2010) 259–269.
[73] A. Villegas-Jimenez, A. Mucci, M.A. Whitehead, Theoretical insights into the hydrated (10.4) calcite surface: structure, energetics, and bonding relationships, Langmuir 25 (2009) 6813–6824.
[74] N.H. de Leeuw, S.C. Parker, Surface structure and morphology of calcium carbonate polymorphs calcite, aragonite and vaterite: an atomistic approach, J. Phys. Chem. B 102 (1998) 2914–2922.
[75] J.H. Lee, A.S. Madden, W.M. Kriven, A.C. Tas, Synthetic aragonite ($CaCO_3$) as a potential additive in calcium phosphate cements: evaluation in Tris-free SBF at 37 °C, J. Am. Ceram. Soc. 97 (2014) 3052–3061.
[76] F. Monchau, A. Lefevre, M. Descamps, A. Belquin-Myrdycz, P. Laffargue, H.F. Hildebrand, In vitro studies of human and rat osteoclast activity on hydroxyapatite, β-tricalcium phosphate, calcium carbonate, Biomol. Eng. 19 (2002) 143–152.
[77] R.F. Dill, L.S. Land, L.E. Mack, H.P. Schwarcz, A submerged stalactite from Belize: petrography, geochemistry, and geochronology of massive marine cementation, Carbonates Evaporites 13 (1998) 189–197.
[78] P. Cubillas, S. Koehler, M. Prieto, C. Chairat, E.H. Oelkers, Experimental determination of the dissolution rates of calcite, aragonite, and bivalves, Chem. Geol. 216 (2005) 59–77.
[79] U. Brand, Strontium isotope diagenesis of biogenic aragonite and low-Mg calcite, Geochim. Cosmochim. Acta 55 (1991) 505–513.